Lamellar grains distribution and plastic strain heterogeneities in TiAl cast samples. Experiments and modelling

Lionel Gélébart, Michel Bornert, Thierry Bretheau, Daniel Caldemaison, Jérôme Crépin, André Zaoui

Lamellar grains distribution and plastic strain heterogeneities in TiAl cast samples. Experiments and modelling

L. Gélébart[2], **M. Bornert**[1], **T. Bretheau**[1], **D. Caldemaison**[1], **J. Crépin**[1], **A. Zaoui**[1]

1 Laboratoire de Mécanique des Solides, (UMR CNRS 7649), Ecole Polytechnique, 91128 Palaiseau cedex, France

2 Service de Recherche en Métallurgie Appliquée, CEA Saclay, 91121 Gif sur Yvette, France

DISTRIBUTION DES GRAINS LAMELLAIRES ET HÉTÉROGÉNÉITÉ DE DÉFORMATION PLASTIQUE DANS DES ALLIAGES DE FONDERIE À BASE TiAl. EXPÉRIENCES ET MODÉLISATION

RÉSUMÉ : Pour certaines conditions de vitesse de refroidissement, les alliages de fonderie à base TiAl présentent une microstructure biphasée [Ti_3Al (α_2) + TiAl (γ)] constituée de petits grains monophasés γ et de grains lamellaires biphasés ($\alpha_2 + \gamma$) ; la distribution radiale des grains lamellaires génère alors une "macrostructure" dont la taille est commensurable à celle des barreaux. D'autre part, à cause de la forte anisotropie de comportement plastique des grains lamellaires (due au peu de systèmes de déformation activable et à l'influence de la morphologie des lamelles), la distribution de la déformation plastique du matériau est fortement influencée par une telle "macrostructure". L'hétérogénéité de déformation au sein du matériau est clairement mise en évidence au moyen d'une mesure de champ de déformation par corrélation d'images appliquée à un essai de compression uniaxial réalisé sur une éprouvette à microstructure radiale. Il découle de cet essai qu'un échantillon avec une telle microstructure ne permet pas de définir un volume élémentaire représentatif du matériau. Il est alors difficile d'évaluer directement des paramètres matériaux tels que cissions critiques, limite d'élasticité, écrouissage, etc.

Afin de remédier à ce problème de non séparabilité des échelles, une approche basée sur un calcul de structure, qui prend en compte la description géométrique de la microstructure radiale ainsi que l'anisotropie de comportement mécanique au moyen d'un critère de Hill isotrope transverse, est présentée. L'optimisation des paramètres du critère de Hill par comparaison avec la réponse expérimentale à la fois à l'échelle macroscopique (courbe de comportement) et à l'échelle locale (champ de déformation) conduit à une meilleure adéquation entre expérience et simulation.

Cette étude met en évidence le risque qu'il y a de ne pas prendre en compte l'agencement de la microstructure : cela conduit à sous-estimer les niveaux de déformation plastique, ce qui pose problème pour des alliages aussi peu ductiles que les alliages à base TiAl.

MOTS CLEFS : Macrostructure, mesure de champ de déformation, TiAl, grains lamellaires

ABSTRACT : During the cooling of TiAl cast alloys, the distribution of the dual-phase lamellar grains [Ti_3Al (α_2) + TiAl (γ)] generates a so-called 'macrostructure'. Because of the highly anisotropic plastic behaviour of the lamellar grains, the distribution of the plastic strain is strongly influenced by such a macrostructure. This heterogeneity is clearly observed by means of a strainfield measurement technique applied to a compression test performed on a cast sample having a 'radial' macrostructure. As a result, a sample having such a macrostructure is not representative of the material and can not be used directly to evaluate 'material parameters'. Moreover the mechanical simulations of cast components should take into account such heterogeneities at the scale of the component. This strong influence is experimentally demonstrated, and a way to take it into account in a mechanical simulation is proposed.

KEYWORDS : Macrostructure, strainfield measurement, TiAl, lamellar grains

During the two last decades, the aeronautic and automotive industry has shown an increasing interest for titanium aluminides (TiAl intermetallic alloys). The main reasons for such an interest are a low density (~3.8), a good stiffness and a high temperature strength up to 750°C. On the other hand, these alloys exhibit, in their polycrystalline form, a poor ductility (4% seems to be an upper bound at room temperature) [1-3] with widely scattered values. One way to improve this type of material could be to optimize the microstructure; thus it seems important to understand its influence on the occurence of plastic strain heterogeneities leading to crack initiations.

The material under study is a cast alloy with a nearly fully lamellar microstructure. Three different scales can be used to describe and study this material: the scale of the lamellae (a few μm), the scale of the lamellar grains (a few mm), and the scale of the sample (a few cm). The last scale describes the organisation of the lamellar grains created during the cooling of the billets.

In the following, these scales are used to describe the material. Then, the study is focused on the "scale of the sample" in order to show that the organisation of the lamellar grains has an important effect on the plastic strain distribution. A way of modelling this type of microstructural organisation is finally proposed and applied to a finite element simulation.

Description of the microstructure

The material has a $TiAl_{48}Cr_2Nb_2$ (at.%) composition and has been cast in billets with a length of 100 mm and a diameter of 20 mm. The resulting microstructure is nearly fully lamellar [Ti_3Al (α_2) + TiAl (γ)] with a low volume fraction (~ 10%) of small equiaxed monophasic γ grains. Thus, the following description is mostly focused on the lamellar phase and its distribution.

The scale of the lamellae

This scale has been extensively investigated. The reported studies, performed by means of Transmission Electron Microscopy, address the different crystalline phases [4], the orientation relationships between lamellae [5], and the deformation mechanisms [6].

Structure and deformation mechanisms of the lamellar phase

The lamellar phase forms during the cooling of the α phase. It is the result of the decomposition of the α phase (an hexagonal compact structure, type A_3) in α_2 and γ phases. In one lamellar grain, all the α lamellae have the same orientation, and the γ lamellae have 6 possible orientations.

The γ phase [4] has a $L1_0$ structure. It is a tetragonal structure (with c/a ratio ~1.015) very close to an F.C.C. structure, with an alternating stacking of titanium and aluminium atomic planes. Many studies on the deformation mechanisms of the lamellar phase have been realised on so-called Poly-Synthetically Twinned (PST) crystals, which can be considered as "single crystals" of lamellar phase. Such crystals have been submitted to tension and compression for different loading axis orientations [6, 7].

The observed mechanisms in γ lamellae are:

- 4 systems {111}<1-10] of ordinary dislocations,
- 4 twinning systems of type {111}<11-2],
- and 8 systems {111}<-101] of superlattice dislocations.

The α_2 phase [4] has a $D0_{19}$ structure. It results in the ordering of the α phase and the c/a ratio is equal to 0.8. A single crystal of a $D0_{19}$ compound with an off-stoichiometric composition (Ti-36.5at.Al), close to the composition of α_2 phase present in lamellar structures, has been studied [8]; the deformation mechanisms are the following:

- 3 prismatic slip systems {1-100}<11-20>,
- 3 basal slip systems (0001)<11-20>,
- and 6 pyramidal slip systems {11-21}<-1-126>.

A lamellar grain can be described (fig. 1) as the stacking of seven different types of lamellae: the α_2 lamellae with the basal plane parallel to the lamellar interface and 6 γ lamellae in crystallographic relation with the α_2 lamellae: the $[110]_\gamma$ direction is parallel to a $<11\text{-}20>_{\alpha_2}$ direction and the $(111)_\gamma$ plane is parallel to the basal plane $(0001)_{\alpha_2}$. The 6 γ lamellae deduce from each others by a rotation of $k\pi/3$ (k = 0,...,6) around $[0001]_{\alpha 2}$.

The strong anisotropy of the lamellar phase

Tensile tests performed on PST crystals [7] for different loading axis orientations have shown a very strong plastic anisotropy (fig. 2). Such an anisotropy can not be only reproduced by choosing different appropriate values for the CRSS (Critical Resolved Shear Stress) of the different types of mechanisms. The role of the interfaces as barriers for the transmission of glide [9] must be accounted for, similarly to what is done with the Hall-Petch law. A "morphological" classification (fig. 3) of the slip systems is then derived [10]: a mechanism is called *Longitudinal* if its slip plane is parallel to the interfaces, *Transverse* if its slip direc-

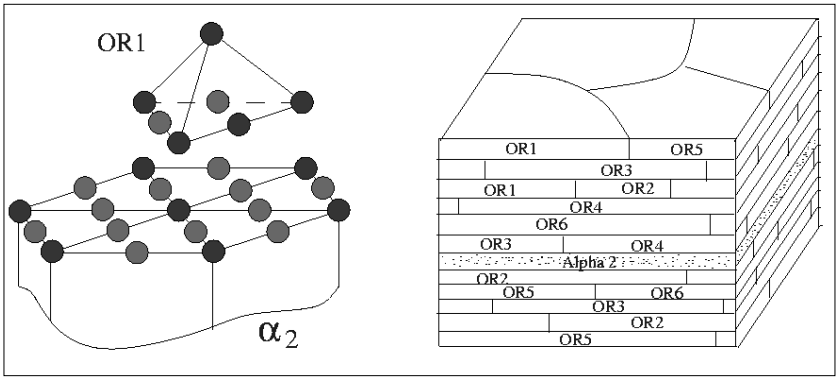

Fig. 1 - Description of the lamellar structure.

Fig.1 - Description de la structure lamellaire.

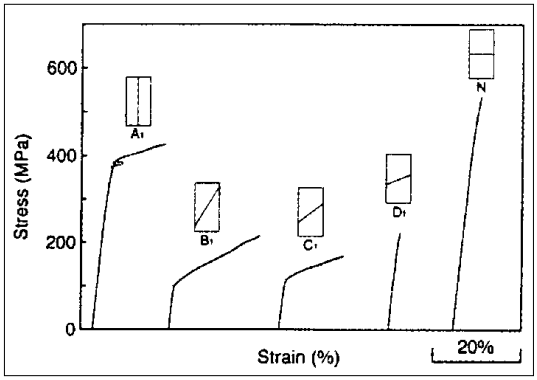

Fig. 2 - Anisotropic behaviour of the lamellar structure [7].

Fig. 2 - Comportement anisotrope de la structure lamellaire [7]

tion and its slip plane are not parallel to the interfaces, and *Mixed* if its slip direction is parallel to the interfaces but its slip plane is not. Of course, for a same type of slip system, the CRSS will be the smallest for a Longitudinal morphology, and the highest for a Transverse one.

The scale of the lamellar grains

This scale will be used to describe the misorientations between lamellar grains and to study the interactions between misoriented grains. As the plastic anisotropy is important, high plastic strain incompatibilities can be expected, that could generate strong stress concentration and explain, partly, the initiation of cracks and the poor ductility of the polycrystalline material. This question which is not the purpose of the present work is presented in [11].

The scale of the sample

While cooling a cast billet, lamellar grains grow radially from the periphery towards the center along the direction of the heat flux. In this radial organisation, the lamellar interfaces are tangentially distributed (fig. 4). Such an heterogeneity, at the scale of the sample, has as consequence that the sample tested is not representative of the 'material' behaviour and all the macroscopic results obtained on such a sample **cannot be used directly** to evaluate material parameters. Moreover the mechanical simulations of cast components should take into account such heterogeneities at the scale of the component. This strong influence is experimentally demonstrated in the next part, and a way to take it into account in a mechanical simulation is proposed in the last one.

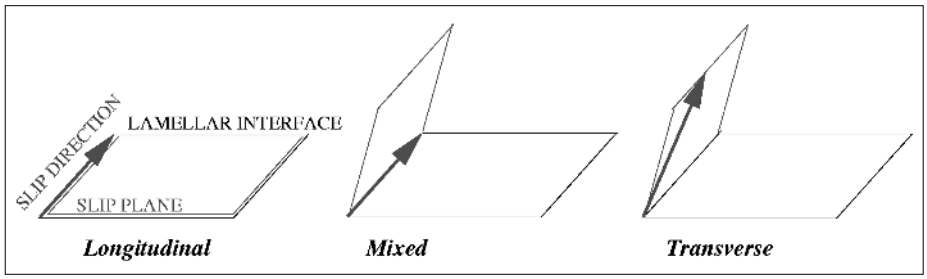

Fig. 3 - "Morphological" classification of the strain mechanisms.

Fig. 3 - Classification "morphologique" des mécanismes de déformation

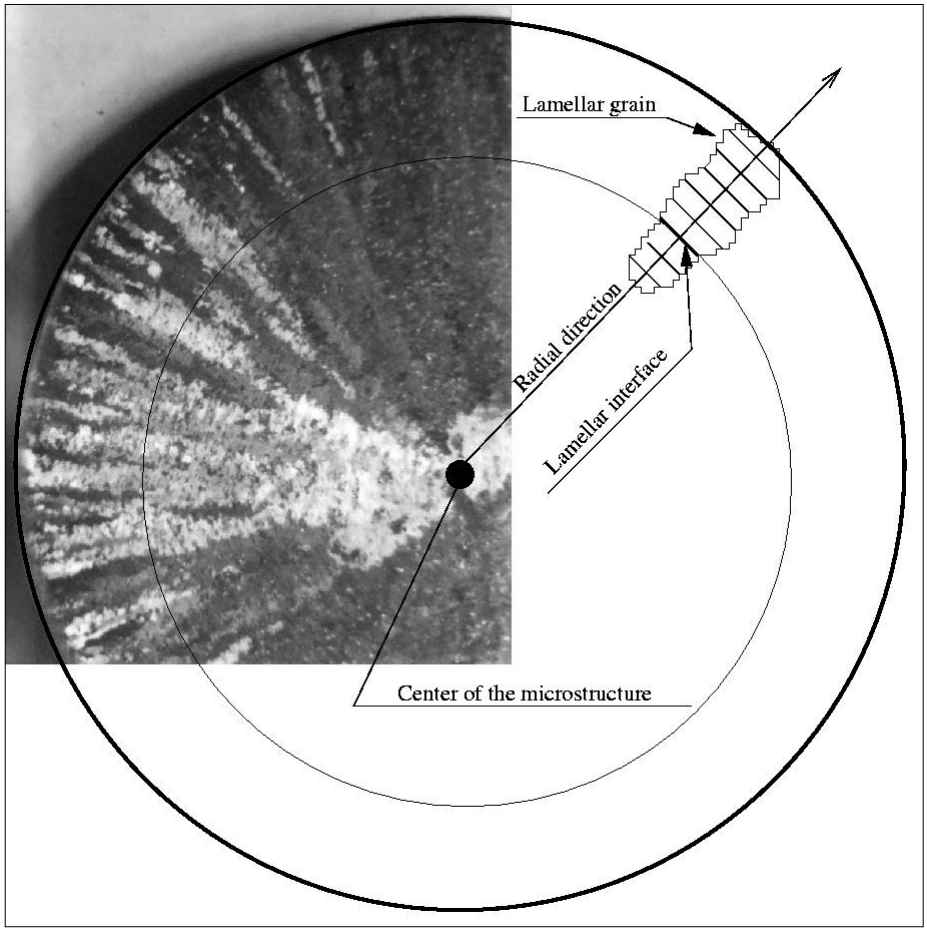

Fig. 4 - Micrograph of the billet's cross section (diameter = 20 mm).

Fig. 4 - Micrographie d'une section transverse du lingot (diamètre = 20 mm).

Experimental study

In order to show the influence of the radial organisation of the lamellar phase, a compressive test is performed with the compression axis along a radial direction of the billet. The strain distribution is investigated by means of a strain field measurement technique.

Strain field measurement technique [12]

The procedure is based on the comparison between digital images of the surface, before and after deformation, corresponding to the reference and the deformed configuration. A virtual grid of reference points is defined on the reference configuration and using classical correlation techniques [12-15] the position of each reference point is found in the deformed configuration. The correlation relies on a contrast provided by a black on white speckle realised on the surface of the specimen

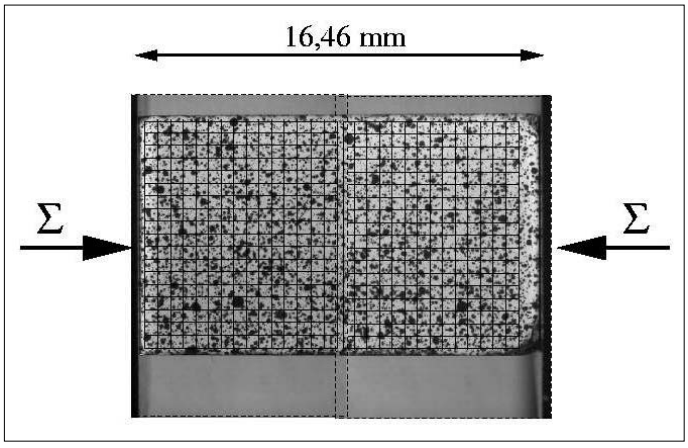

Fig. 5 - Black and white speckle and virtual grid of reference points.

Fig. 5 - Speckle en noir et blanc avec grille virtuelle des points de référence.

(fig. 5). So, the in-plane displacement components and then the in-plane strain field components can be evaluated. The spatial resolution of the method is defined by the choice of the perodicity of the virtual grid of reference points.

Sample

The sample is cut such that the compression axis is along a radial direction of the billet, and such that the center of the macrostructure nearly corresponds to the center of the sample (fig. 6). As the natural contrast of the surface is not sufficient for the correlation method to work efficiently, an artificial marking of the surface has to be done.

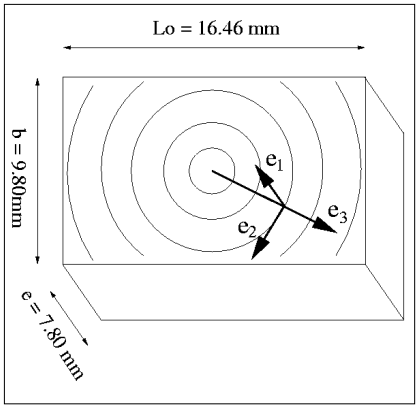

Fig 6 - Description of the sample geometry and axes definition.

Fig. 6 - Description de la géométrie de l'échantillon et définition des axes.

Image acquisition and local strain measurement

A conventionnal CCD camera (Sony SSC M370CE) associated with a 50 mm focal length lens (Pentax) and appropriate extension rings, a computer with an acquisition card (Data Translation) and the software *NIH image* (from the National Health Institute), are used for the acquisition of digital images. To ensure a sufficient local resolution two images are taken to cover the full sample. The images are digitized in 738 × 512 pixels on a grey scale of 256 levels. To reduce the background noise, the image is the result of the averaging of 16 frames. The virtual grid of points defined on the images (fig. 5) has a periodicity of 0.5 mm, leading to a gage length of 1 mm for the local strain measurement, since the deformation gradient components at a given point are estimated from the displacement of the 8 neighbouring points [13]. The strain components are computed under the assumption that the out-of-plane displacement can be neglected, which is a reasonable assumption for the small strains under consideration. In the following, the intensity of the strain will be given by the equivalent strain ε^{eq} ($\varepsilon^{eq} = \sqrt{2/3\ \mathrm{dev}(\underline{\varepsilon}) : \mathrm{dev}(\underline{\varepsilon})}$), where $\mathrm{dev}(\underline{\varepsilon})$ is the deviatoric part of the strain tensor.

Compression test

The compression test is performed with an Instron machine under a macroscopic strain rate of 10^{-4} s^{-1}. The force transducer has a full scale of ±50 kN with a gain of 5 kN/V. As the microstructure presents a strong heterogeneity at the scale of the sample, it has been decided to use a displacement transducer between the crosshead and the fixed platen of the testing machine, rather than a strain gauge. The displacement transducer (LVDT) has a full scale of 10 mm with a gain of 4.09 mm/V. The test is performed sequentially, images being registered at each stage. Four stages are considered : three during the loading, and the fourth one after the elastic unloading.

The experimental response

The macroscopic behaviour is presented on figure 7 and the strain distribution and its evolution from one stage to another, is shown on figure 8, where the equivalent strain is represented on a grey scale from 0 % to 10 %. From the analysis of these strain maps different conclusions can be drawn:

The strain distribution is very heterogeneous at the scale of the sample. As a consequence, the macroscopic response given on figure 7 has to be considered as the response of a 'structure' and

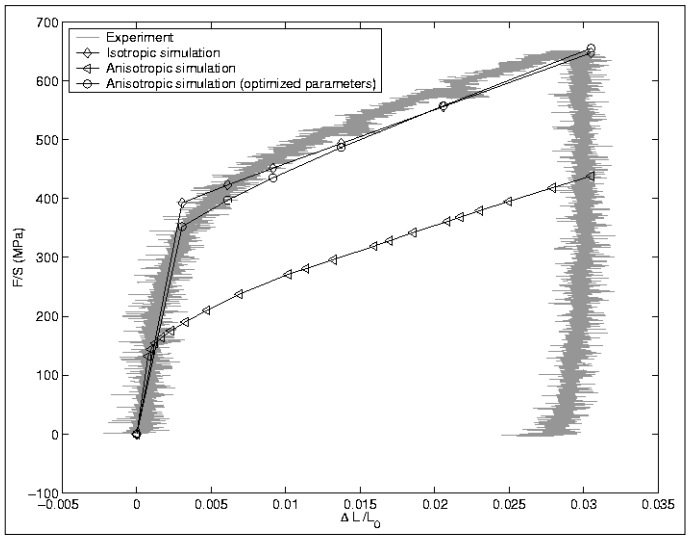

Fig. 7 - Comparison of the global response between the mechanical test and the three numerical simulations.

Fig. 7 - Comparaison de la réponse mécanique globale entre l'essai mécanique et les trois simulations numériques

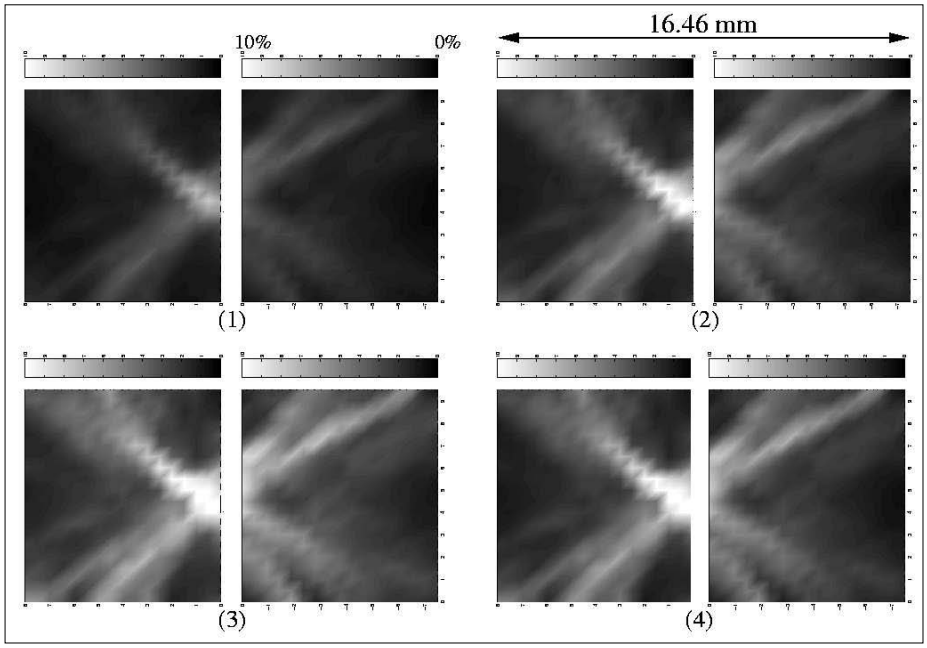

Fig. 8 - Equivalent strain distribution (1) $\Delta l/L_0 = -1.5$ %, (2) $\Delta l/L_0 = -2.2$ %, (3) $\Delta l/L_0 = -3.0$ %, (4) $\Delta l/L_0 = -2.6$ %.

Fig. 8 - Distribution de la déformation équivalente: (1) $\Delta l/L_0 = -1.5$ %, (2) $\Delta l/L_0 = -2.2$ %, (3) $\Delta l/L_0 = -3.0$ %, (4) $\Delta l/L_0 = -2.6$ %.

can not be directly used to evaluate 'material properties' such as the yield stress, the hardening coefficient or any other one.

The strain distribution is strongly linked to the radial organisation of the microstructure. Actually, it can be schematically described by two strain localisation bands and four blocks which are nearly undeformed. The intersection of these bands is exactly positionned at the center of the radial microstructure, which is not exactly the center of the specimen. The position of the two bands can be linked to the orientation of the lamellar grains which have an angle between the compression axis and the lamellar interfaces below 60° and above 30°. Because of the strong anisotropy of the lamellar phase, these orientations are easy to deform (see orientations B1 and C1 on figure 2). On the contrary, the other orientations are harder to deform, and the areas where the grains have such hard orientations correspond to the nearly undeformed four blocks.

The strain distribution remains unchanged when the global deformation increases; only the contrast between the bands and the blocks evolves.

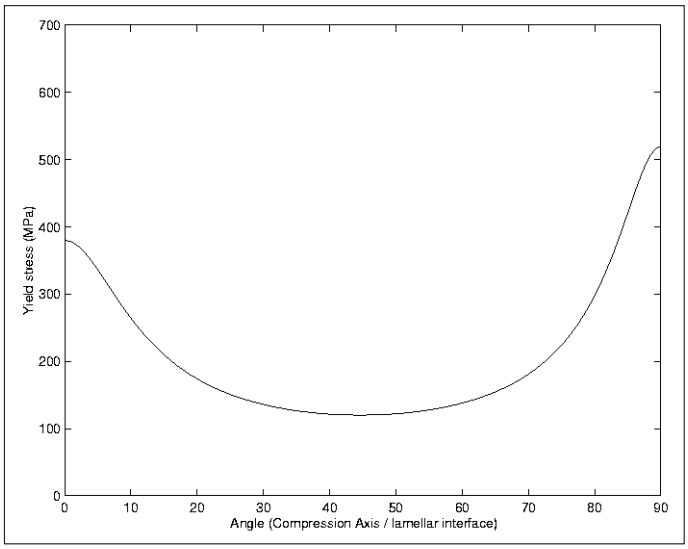

Fig. 9 - Hill criterion fitted on behaviour of the lamellar structure.

Fig. 9 - Critère de Hill ajusté sur le comportement de la structure lamellaire.

A possible model for such 'structures'

As clearly established in the experimental study, the organisation of the microstructure at the scale of the sample has a very strong effect on plastic strain distribution. As a consequence, the question is now to propose a way of modelling such a microstructural organisation to reproduce the local strain distribution as well as the global response obtained experimentally.

The model

The modelling of such a material with an heterogeneity at the scale of the sample is based on two steps of representation. The first one is the definition of local reference axes at each point of the sample and the second is the definition of the behaviour in these local axes. The first step relies on a schematization of the microstructural organisation. In our case, the microstructure is radial what allows us to use cylindrical coordinates with $\underline{e1}$ parallel to the axis of the billet, $\underline{e3}$ the radial direction and $\underline{e2}$ the tangential direction (fig. 6). The second step deals with the local behaviour definition which should take into account the description of the microstructure. A rough description of the microstucture can be used as a first trial: it is assumed to be fully lamellar with the lamellar interfaces exactly tangentially distributed, so that the local behaviour is given by the behaviour of the lamellar phase. It is assumed elasto-plastic, with isotropic elastic properties and the elastic domain defined by a transversal isotropic Hill's criterion ($\underline{e1}$, $\underline{e2}$) being the plane of transverse isotropy. The hardening is supposed to be linear and isotropic. This behaviour is then given by the following relations:

$$\underline{\underline{\sigma}} = \mathrm{K}(\underline{\underline{\varepsilon}} - \underline{\underline{\varepsilon}}^{\mathrm{p}})$$

$$f(\underline{\sigma}) = \sqrt{\sigma_{\mathrm{eqE}}^2 + N\sigma_{\mathrm{eqL}}^2 + L\sigma_{\mathrm{eqT}}^2} - (\sigma_0 + R) = 0$$

$$\dot{R} = h\dot{\varepsilon}_{\mathrm{eq}}^{\mathrm{p}}$$

where $\sigma_{\mathrm{eqE}}^2 = -(2\sigma_{33} - \sigma_{11} - \sigma_{22})^2$, $\sigma_{\mathrm{eqT}}^2 = -[(\sigma_{22} - \sigma_{11})^2 + 4\sigma_{12}^2)$, and $\sigma_{\mathrm{eqL}}^2 = \sigma_{13}^2 + \sigma_{23}^2$.

The elastic coefficients, measured by Schafrik [16], are E = 180 GPa and $\nu = 0.28$. The three coefficients of the Hill criterion are evaluated from the three yield stresses (380 MPa, 120 MPa and 520 MPa) obtained on tensile tests performed on PST crystals [7] with the orientations (0°, 45° and 90°) (fig. 2). With this set of parameters ($N = 6.49$, $L = 73.24$, and $\sigma_0 = 520$ MPa), the evolution of the yield stress as a function of the angle between the tensile axis and the lamellar interface is given figure 9. The hardening coefficient is chosen as h = 7 000 MPa so that the hardening of the simulated global response is in good agreement with the experimental one.

Application to a finite element calculation

In order to show that the contact between the platen and the sample can not lead to the experimental strain distribution, a compression test is simulated assuming that the material is isotropic and homogeneous. Then, the heterogeneous and anisotropic model is taken into account, and finally the modelling is discussed and its parameters are modified in order to improve the comparison between simulation and experiment.

Simulation with an homogeneous and isotropic model

In order to minimize the calculations, and by accounting with the different symmetries of the problem, only one eighth of the specimen is simulated. The dimensions are those of the compression specimen. Quadratic elements with 20 nodes and 27 integration points are used. The boundary conditions (fig. 10) are: symmetry conditions for the faces A, B and C, free surface condition for the faces E and F, the displacements of face D are imposed to zero in X and Y directions, and imposed to −0.25 mm (or $\Delta l/L_0 = -3\,\%$) in Z direction. These boundary conditions for face D represent the

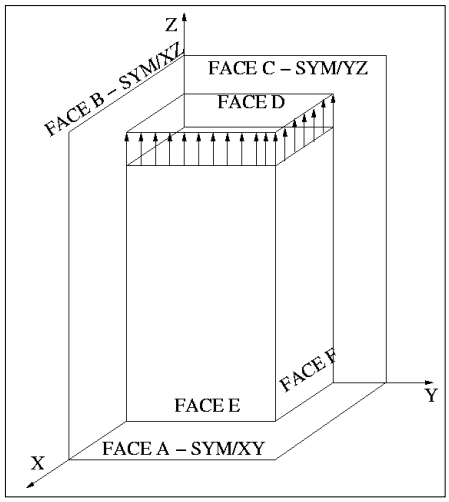

Fig. 10 - Description of the boundary conditions.

Fig. 10 - Description des conditions aux limites.

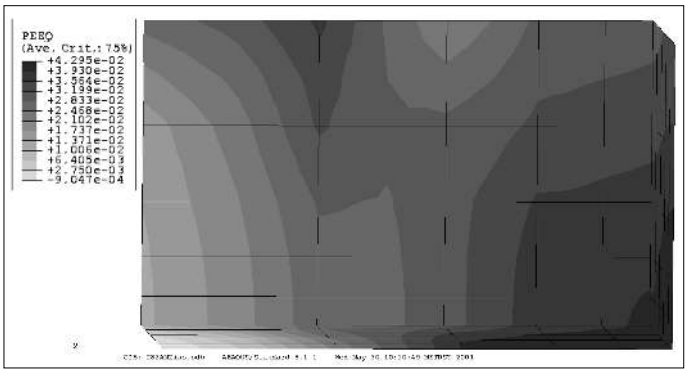

Fig. 11 - Homogeneous microstructure and isotropic modelling. Equivalent plastic strain distribution.

Fig. 11 - Modélisation isotrope pour microstructure homogène. Distribution de la déformation plastique équivalente.

contact between the specimen and the platens of the testing machine, where the strong friction locks any X, Y displacements. As the aim of this first calculation is to evaluate the effect of the contact platens/specimen in the case of a compression test, the material is chosen homogeneous and isotropic. The elasto-plastic behaviour is described by a Von Mises criterion associated to a linear isotropic hardening, the yield stress is chosen equal to 400 MPa and the other parameters are those already mentionned. These values are fitted on the experimental global response (fig. 7). The obtained equivalent plastic strain distribution are presented on figure 11. Two different effects can be attributed to these boundary conditions : the first is a localisation near the edges of the specimen, and the second one is an heterogeneity centered in the middle of the specimen. However such a distribution is too smooth compared to the experimental one (fig.8). So, the boundary conditions can not explain the observed experimental strain distribution, even if they give a small contribution to it.

Simulation with an anisotropic behaviour radially distributed

For this second calculation, the behaviour of the material is the one described in section "The model". For simplicity, the center of the microstructure is supposed to be exactly at the center of the specimen, so that the same symetry conditions as above can be used. The obtained equivalent plastic strain distribution is shown on figure 12. This distribution is qualitatively close to the experimental strain distribution. In order to have a quantitative comparison between the simulation and the experimental results, the equivalent plastic strain is averaged in three particu-

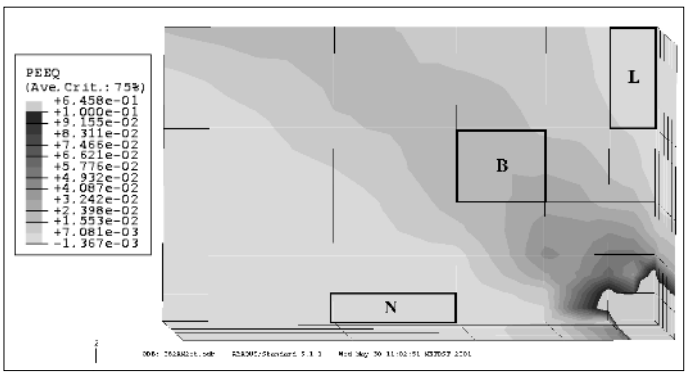

Fig. 12 - Radial microstructure and anisotropic modelling. Equivalent plastic strain distribution.

Fig. 12 - Modélisation anisotrope et microstructure radiale. Distribution de la déformation plastique équivalente.

Table I - Comparison of the experimental and numerical value of the average equivalent strain in element N, L, and B after unloading.

Tableau I - Comparaison de la valeur expérimentale et numérique de la déformation équivalente moyenne pour les éléments N, L, et B après déchargement.

	Element N	**Element L**	**Element B**
ε_{eq} (Experimental value)	2.2 %	1.6 %	4.6 %
ε_{eq} (numerical value)	0.01 %	0.3 %	2.2 %
ε_{eq} (optimized numerical value)	2.0 %	1.9 %	4.0 %

lar elements shown on figure 12. Element N is supposed to be representative of the block where the lamellae are almost normal to the compression axis, element L is representative of the block where the lamellae are almost parallel to the compression axis, and element B is representative of the strain localisation band. The equivalent plastic strains averaged on these elements for $\Delta l / L_0 = -3\,\%$ are compared to the same averages of the experimental equivalent strain measured after elastic unloading (Table I).

This quantitative analysis performed at local scale shows that, despite of a qualitative agreement, the simulation still has to be improved. The same conclusion can be drawn from the global response (fig. 7), which is too soft compared to the experiment. It seems that the localisation in this second calculation is too strong compared to the experiment, especially at the center of the sample.

Discussions and improvements of the simulation

The previous modelling can be seen as the result of a deductive approach where the simulation at the scale of the sample directly takes into account the behaviour of the local constituents, the lamellar grains in our case. The quantitative disagreement observed can find its explanation in the drastic simplification done in the definition of the local behaviour. First, the Hill's criterion used to described the yield surface of the lamellar phase can be different from the real yield surface, even if, at least, it describes correctly the response for tensile tests. Secondly, the local behaviour is fitted on the behaviour of the single lamellar crystal, so it cannot take into account : the misorientations of the lamellar grains compared to the tangential position, the interactions between these misoriented grains, and the role of the small γ grains that can be seen at the boundaries of the lamellar grains. Finally, a fully deductive approach should take into account all these considerations via a polycristalline modelling, leading to a local behaviour that is more isotropic than the behaviour of the lamellar phase. In the following, this fully deductive approach is given up and a more inductive approach is used. To improve the comparison between simulation and experiment, and because of the qualitative agreement of the previous simulation, we suggest to keep the previous modelling (the tangential distribution of a transversal isotropic Hill's criterion), but to modify the parameters to get a more isotropic behaviour. The new set of parameters σ_0 = 500 MPa, N = 4.71, L = 9.68 and h = 6000 MPa) is evaluated so that the global simulated response as well as the local one (the averaged equivalent plastic strains in the elements N, B and L), are in a quantitative good agreement with the experimental responses. The global response is shown figure 7, the equivalent plastic strain distribution is shown figure 13, and the average values on the elements N, L and B are given in table I. With this new set of parameters, the evolution of the yield

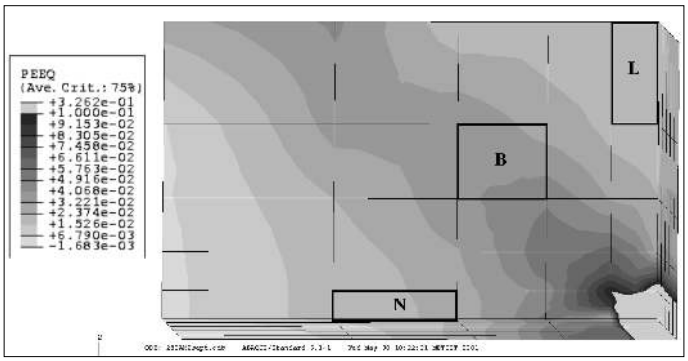

Fig. 13 - Radial microstructure and anisotropic modelling. Equivalent plastic strain distribution. Optimized parameters.

Fig. 13 - Modélisation anisotrope et microstructure radiale. . Distribution de la déformation plastique équivalente. Paramètres optimisés.

stress as a function of the angle between the tensile axis and the lamellar interface is shown figure 14. It can be seen that the new local behaviour is more isotropic than the behaviour of the lamellar phase (figure 9).

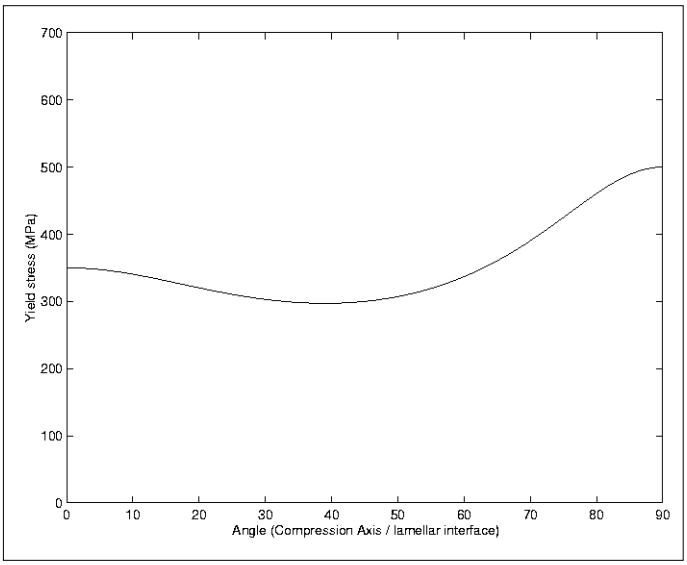

Fig. 14 - Hill criterion with optimized parameters.

Fig. 14 - Critère de Hill avec paramètres optimisés.

Conclusions

Thanks to a strain field measurement technique the influence of the distribution of the lamellar phase in a cast billet, has been shown. This radial distribution leads to a very strong heterogeneity of the plastic strain distribution. As a consequence: a tensile test realised on a sample having such a microstructural distribution cannot be used directly to evaluate material properties, a mechanical simulation realised on a cast component, should take into account such a microstructural distribution.

The strong heterogeneity of plastic strain can be related to the strong anisotropy of the lamellar phase. A simple way of modelling this macrostructure has been proposed. It relies on a transversal isotropic Hill's criterion tangentially distributed. First, the parameters are fitted on the behaviour of the lamellar phase, but the obtained results are just in a qualitative agreement with experiment, the obtained strain field being too heterogeneous. Then, the parameters have been modified to obtain a quantitative agreement. This new set of parameters leads to a more isotropic behaviour, which could be due to the polycristalline interactions which were ignored in the first test. ❑

Acknowledgements

This work is realised in a common project between the french scientific institute CNRS, two industrial firms (SNECMA Moteurs and Turboméca), and six french laboratories (LSG2M in Nancy, CEMES in Toulouse, LTPCM in Grenoble, LMPM in Poitiers, GMP in Rouen, CECM in Vitry and LMS in Palaiseau).

REFERENCES

[1] YAMAGUCHI M., INUI H., KISHIDA K., MATSUMORA M. and SHIRAI Y., *Mat. Res. Soc. Symp. Proc.,* 1995, 364, 3.

[2] KIM Y.W., *JOM*,1994, 30.

[3] GUÉDOU J.Y., *14ème Congrès Francais de Mécanique*, Toulouse, 1999.

[4] DENQUIN A., Thèse de doctorat, Université de Lille, 1994, No 1295.

[5] ZGHAL S., NAKA S. and COURET A., *Acta Materialia*, 1997, 45, 3005.

[6] KISHIDA K., INUI H. and YAMAGUCHI M., *Phil. Mag. A.* 1998, 78, 1.

[7] INUI H., NAKAMURA A., Oh M.H. and YAMAGUCHI M., *Phil. Mag. A,* 1992, 66, 557.

[8] INUI H., TODA Y. and YAMAGUCHI M., *Phil. Mag. A*, 1993, 67, 1315.

[9] INUI H., OH M.H., NAKAMURA A. and YAMAGUCHI M., *Phil. Mag. A,* 1992, 66, 539.

[10] LEBENSHON R., UHLENHUT H., HARTIG C. and MECKING H., *Acta Materialia,* 1998, 46, 4701.

[11] L. GÉLÉBART, thèse de doctorat de l'Ecole Polytechnique, 2002.

[12] SUTTON M. A., WOLTERS W. J., PETERS W. H., RANSON W. F. and MCNEILL S. R., *Image and vision computing*, 1983, 1, 133-139.

[13] ALLAIS L., BORNERT M., BRETHEAU T. and CALDEMAISON D., *Acta Materialia* 1994, 42, 11, 3865-3880.

[14] DOUMALIN P. , thèse de doctorat de l'Ecole Polytechnique, 2000.

[15] SOPPA E., DOUMALIN P., BINKELE P., WIESENDEANGER T., BORNERT M. and SCHMAUDER S., *Proceedings of IWCM9,* Berlin, 1999, *Computational Materials Science*, 2001, 21, 261-275;

[16] SCHAFRIK R.E., *Metal. Trans. A* ,1977, 8A, 1003.